Publishing House
AKAPIT

COMPUTER METHODS IN MATERIALS SCIENCE

Informatyka w Technologii Materiałów

Vol. 12, 2012, No. 3

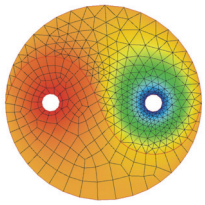

PHYSICAL SIMULATION OF THERMOMECHANICAL PROCESSING OF NEW GENERATION ADVANCED HIGH STRENGTH STEELS

ADAM GRAJCAR[1]*, ROMAN KUZIAK[2], WOJCIECH OZGOWICZ[1], KLAUDIUSZ GOŁOMBEK[1]

[1]Silesian University of Technology, Institute of Engineering Materials and Biomaterials, Gliwice, Poland
[2]Institute for Ferrous Metallurgy, Gliwice, Poland
**Corresponding author: adam.grajcar@polsl.pl*

Abstract

The scientific aim of the paper is the comparative analysis of the hot-working behaviour and microstructure evolution of thermomechanically processed and controlled cooled three advanced high-strength steels (AHSS) used in the automotive industry. The hot workability of three selected steel grades with a various content of Mn and C being major austenite-forming elements was compared. Evaluation of the resistance for hot deformation was carried out on a basis of continuous compression, double-hit compression, four-step compression and seven-step compression experiments simulating conditions similar to industrial processes. It was found that the hot workability of the new generation of AHSS is very challenging due to high values of flow stresses required. However, it is possible to obtain fine-grained transformation products of supercooled austenite with a high volume fraction of retained austenite for low-alloyed steels or single-phase austenitic microstructure in the high-manganese steel. Thermally activated processes of microstructure restoration which enable for successive grain refinement and affecting final flow stress values were identified. Finally, the comparison of the microstructures characterizing the first, second and third generation of AHSS was carried out. Some similarities and differences concerning the hot deformation behaviour and microstructure detailes are indicated.

Key words: physical simulation, thermomechanical processing, AHSS steel, TRIP steel, bainitic steel, high-Mn steel, multiphase steel, retained austenite

1. INTRODUCTION

Significant development of new steel grades for the automotive industry has been made in the period of the last twenty years. From the aspect of materials, this development has been accelerated by strong competition with non-ferrous aluminium and magnesium alloys as well as with polymer composites, which significance has been successively increasing. From the aspect of ecology, an essential factor is to limit the amount of exhaust gas emitted to the environment. It is strictly related with fuel consumption, mainly dependent on a car weight. Application of sheets with lower thickness, preserving proper stiffness, requires application of steel sheets with higher mechanical properties, keeping adequate technological formability. Figure 1 presents schematically the relation between strength properties and ductility of three generations of advanced high strength steels (AHSS) used in the automotive industry. They cover a very wide range of mechanical and technological properties and are at a different level of their industrial application. Multiphase steels belonging to the 1st generation of AHSS are industrially produced as cold-rolled or hot-rolled sheets. However, there is a need to further increase their strength level without

 ISSN 1641-8581

deterioration of ductility as well as there are still many problems to solve with their technological formability, joining, etc. The 2nd generation of AHSS and 3rd generation of AHSS are presently at a phase of intense world-wide research covering various aspects of physical metallurgy, metal forming, joining, modelling, etc. Physical simulation of microstructure evolution of multiphase steels during thermomechanical processing is one of the challenges to solve.

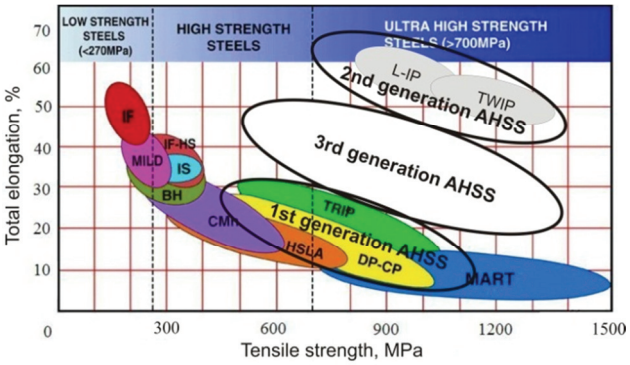

Fig. 1. *Schematic showing of relation between total elongation and tensile strength for different grades of advanced high strength steels (AHSS) for automotive industry; 1st generation AHSS (DP, TRIP, CP, MART), 2nd generation AHSS (L-IP, TWIP) (Speer et al., 2011).*

2. MICROSTRUCTURE AND PROCESSING OF ADVANCED HIGH STRENGTH STEELS

1st generation of AHSS covers different ferrite-based steels. Their mechanical properties and technological formability are dependent on relative proportions and mechanical properties of individual microstructural constituents (Adamczyk & Grajcar, 2007; Ehrhardt & Gerber, 2004; Kuziak et al., 2008). In this regard, their mechanical behavior can be compared to composite materials consisting of a matrix and reinforcing components. Ferrite forms a matrix of AHSS whereas the strengthening phases are martensite and/or bainite. The technological formability of steel sheets decreases and strength properties increase together with an increasing fraction of a hard microstructural constituent. In this way, Interstitial Free (IF) and Bake Hardenable (BH) steels characterized by a uniform ferritic microstructure (not taking into account disperse particles) posses the highest ductility (figure 1). IF and BH sheet steels with moderate strength and high susceptibility to deep drawing are used mainly for elements of body panelling. A growth of strength properties can be obtained in Dual Phase (DP) steels consisting of a ferrite matrix and uniformly distributed martensitic or martensitic-bainitic islands (Kuziak et al., 2011; Kuziak & Pietrzyk, 2011). The further rise of strength is possible to obtain for steels with a ferritic matrix containing bainitic-austenitic islands, where final mechanical properties are formed during cold working under conditions of strain-induced martensitic transformation of metastable retained austenite (ca. 10-15 vol.%). This phenomenon results also in the additional increase of plasticity due to delaying necking and it is called TRansformation Induced Plasticity (TRIP) effect (Bleck & Phiu-On, 2005; Eberle et al., 1999; Grajcar, 2007a). Complex Phase (CP) steels with fine-grained ferrite containing disperse particles of MX-type phases and increased fractions of bainite and martensite as well as low-carbon martensitic steels (MS) show highest strength properties but the lowest ductility. These steel sheets can be used for different reinforcing elements of a car structure.

Multiphase steel sheets are produced by continuous annealing of cold-rolled sheets (Eberle et al., 1999; Kuziak et al., 2011; Kuziak & Pietrzyk, 2011) or they are thermomechanically hot-rolled and controlled cooled (Grajcar, 2007b; Suwanpinij et al., 2012) dependent on the chemical composition, initial microstructure and their application. Physical simulation and mathematical modeling of cold-rolled and continuously annealed multiphase steels are described in detail by Kuziak et al. (2011) and Molenda et al. (2010). The present work is focused on hot-rolled multiphase steels. Anyway, the schematic drawing of heat treatment after cold rolling for TRIP-type steel is shown in figure 2. The temperature between A_{c3} and A_{c1} determines relative fractions of austenite and ferrite and a carbon content in γ phase. DP steels are quenched from an intercritical temperature range to form martensite islands in a ferritic matrix whereas TRIP steel are isothermally held at a bainitic transformation range to enrich austenite in carbon (figure 2). Temperature-time parameters of isothemal holding are crucial for stabilization of the required amount of retained austenite (Grajcar, 2007b; Siodlak et al., 2008).

A ferrite fraction of hot-rolled steels depends on finishing rolling conditions and a cooling path at a region of the γ→α transformation (figure 3) as distinct from cold-rolled sheets. Further cooling on the run-out table is similar to cold-rolled sheets. Isothermal holding of hot-rolled steel sheets takes place during sheet coiling. Its goal is to enrich austenite in carbon to a content ensuring lowering the martensite

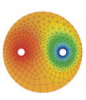

start temperature $M_{s\gamma}$ below room temperature. Finally, TRIP steels contain ferrite as a matrix and bainitic-austenitic islands.

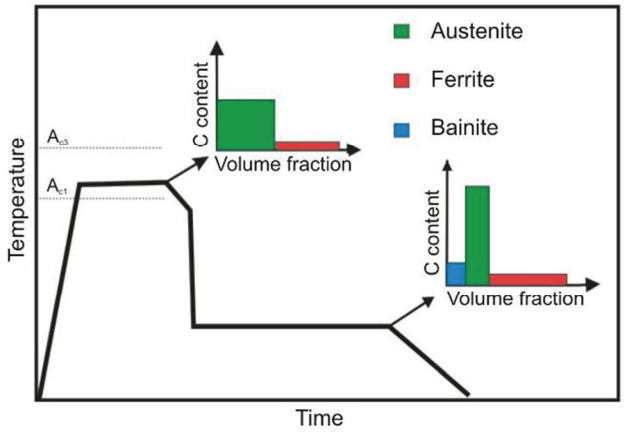

Fig. 2. *Schematic drawing of the heat treatment for TRIP-type steel after cold rolling together with carbon content changes for individual microstructural constituents.*

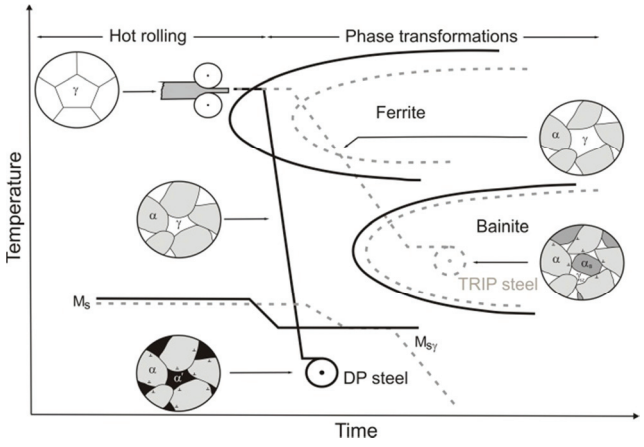

Fig. 3. *Cooling paths used for DP (solid line) and TRIP (dotted line) steels to obtain a desired multiphase microstructure after hot rolling (Bleck & Phiu-On, 2005).*

A prerequisite to produce hot-rolled sheets with required microstructures, including in particular a large fraction of ferrite, is an adequate selection of chemical composition of steel assuring a proper shape of supercooled austenite transformation diagrams CCT with the γ→α transformation put forward to short times and γ→bainite transformation shifted in the opposite direction (figure 4). Shifting the γ→α transformation towards short time occurs along with increasing concentration of Si, Al and P in steel, and γ→bainite transformation in the opposite direction together with increasing amount of C, Mn and Cr. Especially important is to avoid a pearlitic transformation, what is realized by Mn, Mo, Ni and Al alloying.

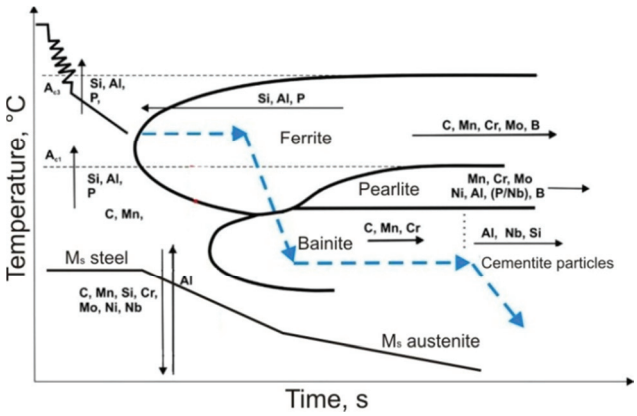

Fig. 4*. Scheme of the influence of alloying elements on the continuous cooling transformation diagram with a cooling path typical for TRIP-type sheets after hot rolling (Ehrhardt & Gerber, 2004).*

2nd generation of AHSS. Nowadays, apart from limiting fuel consumption, special emphasis is placed on increasing the safety of car users (Gronostajski et al., 2010). The role of structural elements such as frontal frame members, bumpers and other parts is to take over the energy of an impact. Therefore, steels that are used for these parts should be characterized by high product of UTS and UEl, proving the ability of energy absorption. These requirements of the automotive industry can be met by the 2nd generation of AHSS combining exceptional strength and ductility as well as cold formability (figure 1). These TWIP (Twinning Induced Plasticity) and L-IP (Light – Induced Plasticity) steels belong to a group of high-manganese austenitic alloys but are much cheaper comparing to Cr-Ni stainless steels. Their main advantage over first generation steels with a matrix based on A2 lattice is the great susceptibility of austenite to plastic deformation, during which dislocation glide, mechanical twinning and/or strain-induced martensitic transformation can occur.

The group of high-manganese steels includes alloys with 15-30% Mn content. Mechanical properties of high-manganese steels are dependent on structural processes occurring during cold deformation, which are highly dependent on SFE (stacking fault energy) of austenite (Dobrzański et al., 2009; Grajcar et al., 2009; Opiela et al., 2009). In turn, the SFE is dependent on the temperature and chemical composition. Figure 5 shows that the stacking fault energy increases with increasing temperature and Al, Cu content whereas Cr and Si decrease it. If the SFE is from 12 to 20 mJm^{-2}, a partial transformation of austenite into martensite occurs as a main deformation mechanism, taking advantage of TRIP effect. Values of SFE from 20 to 60 mJm^{-2}

determine intense mechanical twinning related to TWIP effect. At SFE values higher than about 60 mJm^{-2}, the partition of dislocations into Shockley partial dislocations is difficult, and therefore the glide of perfect dislocations is the dominant deformation mechanism. In TRIPLEX steels with a microstructure of austenite, ferrite and κ-carbides ($(Fe,Mn)_3AlC$) and for SFE > 100 mJm^{-2}, the SIP (Shear Band Induced Plasticity) effect is considered as the major deformation mechanism (Frommeyer & Bruex, 2006).

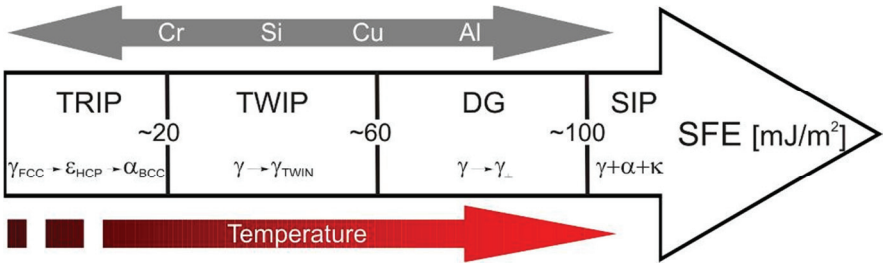

Fig. 5. *Schematic drawing of the effects of temperature and chemical composition on the stacking fault energy (SFE) of austenite and the correlation of SFE with a major deformation mechanism in high-Mn alloys.*

High-manganese steel sheets are usually produced by hot rolling followed by slow air cooling to coiling temperature. The thermomechanical processing combined with direct solution heat treatment from a finishing deformation temperature can be also applied (Dobrzański et al., 2009; Grajcar et al., 2009).

3rd generation of AHSS. In spite of excellent mechanical properties of high-Mn austenitic steels belonging to the 2nd generation of AHSS their application will be probably limited only for most challenging auto-body elements, for example, specially geometrically-designed sections absorbing energy during crash events. The reasons are different technological problems related to poor castability, hot-working above 1150°C, corrosion resistance, Mn segregation and especially the high cost due to Mn (between 20 and 30 wt.%), Al and Si alloying. The idea of the 3rd generation of AHSS is to obtain mechanical properties between the 1st generation and 2nd generation of AHSS at cost just slightly higher compared to the 1st generation low-alloyed multiphase steels (Speer et al., 2011). These steels utilize composite-like behavior of various phases (martensite, non-carbide bainite, fine-grained ferrite, retained austenite) to obtain the desired level of mechanical properties and technological formability. The final combination of high-strength and ductility is possible to obtain by complex interaction of different structural processes, including: solid solution hardening, precipitation hardening, microalloying, grain refining and TRansformation Induced Plasticity (TRIP) or TWinning Induced Plasticity (TWIP) effects.

One of the chemical composition concepts to obtain a bainitic matrix containing a high volume fraction of metastable retained austenite is Mn alloying but to a much lesser extent than in high-Mn steels of the 2nd generation AHSS. Manganese is a main austenite stabilizer and its content reaches up to 7 wt.% in recently investigated C-Mn-Al-Si steels (Grajcar et al., 2012). Increased hardenability of steel due to Mn alloying leads to considerable decrease in a ferrite fraction as a result of shifting the $\gamma \rightarrow \alpha$ transformation field to the right side on CCT diagrams. A heat treatment for steels with increased Mn content is similar to that used for DP and TRIP steels, i.e., intercritical annealing after cold rolling or intercritical annealing and isothermal holding at a bainitic transformation range. The thermomechanical processing, microalloying with Nb, Ti, V, reverse martensite transformation and quenching and partitioning (QP) processing are the examples of ideas to obtain fine-grained complex microstructures with a high fraction of austenitic phase of optimal stability for strain-induced martensitic transformation during drawing, stretching, bending, etc. (Grajcar et al., 2012; Speer et al., 2011; Thomas et al., 2011).

3. MODELS DESCRIBING THE MICROSTRUCTURE EVOLUTION OF THERMOMECHANICALLY-PROCESSED AUTOMOTIVE STEELS

Thermomechanical processing of AHSS still represents a new challenge due to a lack of enough data on their hot deformation resistance and microstructure evolution during multi-step controlled cooling. Thermomechanical treatment can be effectively modelled by physical simulation methods reflecting complex industrial temperature-time-strain cycles using small samples in metallurgical process simulators (Hadasik et al., 2006; Kuziak, 2005). So far, the integration of physical simulation and numerical models enabled developing of industrial technologies for HSLA and IF steels (Kuziak, 2005; Majta et al., 1998; Militzer, 2000; Niżnik & Pie-

trzyk, 2011; Uranga et al., 2007). At present, the intense research activities are carried out to elaborate the complex thermomechanical rolling schedules for DP, TRIP, CP and QP steel sheets – where besides hot-working behavior – models of phase transformations of deformed austenite are needed (Kuziak et al., 2011; Liu et al., 2007; Molenda et al., 2010; Pietrzyk et al., 2010; Suwanpinij et al., 2012; Thomas et al., 2011).

The initial steps of the physical and numerical simulation of the thermomechanical processing of AHSS include modeling of microstructure evolution of deformed austenite. It requires taking into account many equations describing recovery, recrystallization and grain growth processes. Models of strain-induced precipitation of various carbonitrides in austenite affecting a recrystallization kinetics and the austenite grain size evolution have to be also applied in microalloyed steels. Generally, the output parameters of hot-working modeling are the final austenite grain size and residual strain describing the degree of austenite pancaking. These modeling problems using various techniques (thermodynamic models, rheological models, cellular automata, inverse analysis, multiscale modeling, etc.) are well described in the literature (Hadasik et al., 2006; Kuc & Gawąd, 2011; Majta et al., 1998; Militzer, 2000, 2007; Militzer et al., 2000; Molenda et al., 2010; Niżnik & Pietrzyk, 2011; Uranga et al., 2007) and will not be repeated here.

The crucial problem for modeling of AHSS microstructure evolution is decomposition of pancaked austenite during run-out table cooling and following coiling. The austenite decomposition models follow the concept of a sequential transformation model with sub-models for transformation start, ferrite growth, bainite start, bainite growth and martensite formation (Liu et al., 2007). Ferrite transformation start is usually described by a model considering early growth of corner nucleated ferrite. A fraction of austenite transformed into ferrite is predicted by the Johnson-Mehl-Avrami-Kolomogorov (JMAK) model in combination with Scheil's equation of additivity (Kuziak & Pietrzyk, 2011; Liu et al., 2007; Militzer, 2007). A further microstructure evolution model requires the determination of bainite or martensite start temperatures depending on a steel grade (TRIP-type or DP-type). A fraction of undercooled austenite, which transforms into martensite in DP steels can be calculated from the model of Koistinen and Marburger (1959):

$$X_m = 1 - exp\,[-0.011(T_M - T)] \qquad (1)$$

where: X_m – volume fraction of martensite with respect to the whole volume of austenite, which remains at T_M.

The most advanced phenomenological model describing the bainite transformation and retained austenite amount in TRIP steels was developed by Liu et al. (2007). To describe the kinetics of the bainite evolution, a diffusional approach was adopted. The growth rate of a bainitic ferrite plate was calculated using the Zener-Hillert equation in which the interfacial carbon content of austenite is determined taking into account the Gibbs-Thomson effect (Liu et al., 2007). The initially developed model was satisfactory except the prediction of carbide precipitation influencing the amount and stability of retained austenite. Main discrepancies are a result of some difficulties in description of the bainitic transformation. Figure 6 shows a complex character of the bainitic transformation which can proceed with carbide precipitation or without it. In Si- or Al-containing TRIP steels the second option is privileged but it is not a rule due to variations in chemical composition and/or process parameters. As a result, various morphological forms of bainite such as, granular bainite, degenerate upper bainite, degenerate lower bainite, can form (figure 6) depending on a chemical composition concept, cooling rate and coiling temperature (Zajac et al., 2005).

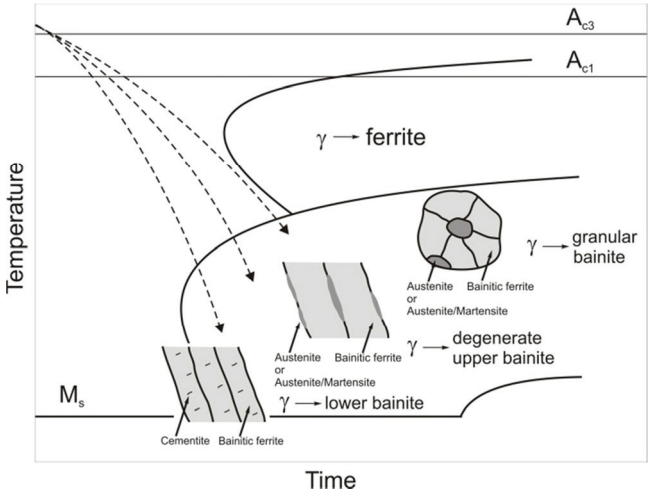

Fig. 6. *CCT diagram with various morphological types of bainite depending on a cooling rate from an austenite region.*

The recent most advanced model of formation of bainitic ferrite and carbides in TRIP steels was developed by Fazeli and Militzer (2012). A nucleation-growth based model was used to describe the simultaneous formation of bainitic ferrite and cementite precipitation. Nucleation and growth equations for cementite and bainitic ferrite were coupled and the carbon content of austenite was determined from the

balance of C enrichment due to bainite formation and C depletion due to Fe_3C precipitation.

4. EXPERIMENTAL PROCEDURE

The paper addresses the comparison of the physical simulation of thermomechanical processing and microstructure evolution of three generations of advanced high strength steels. Three model steel grades belonging to the 1st generation, 2nd generation and 3rd generation of AHSS were selected to compare their hot-working behavior, cooling procedures and final microstructures. The chemical composition of the investigated steels and their designation are given in table 1. Detailed information on the chemical composition strategy can be found in earlier works (Grajcar, 2007b; Grajcar et al., 2009, 2012). The total content of alloying elements (Mn+Al+Si+Mo) is equal to about 2.8, 29.5 and 5 wt.%, respectively for the 1st, 2nd and 3rd generation steels. It is worth to note that the low-alloyed steels are characterized by the high metallurgical purity (low contents of S and P) whereas the high-Mn steel contains some increased sulphur content added to the melt together with electrolytic Mn charge.

The steels were made by vacuum induction melting in the Balzers VSG-50 furnace in the Institute for Ferrous Metallurgy, Gliwice. Liquid metal was cast in the argon atmosphere into a cast iron mould. Homogenization treatment at 1200°C for 4 hours (high-Mn steel) or 3 hours (low-alloyed steels) was carried out to remove the segregation of alloying elements (especially Mn). Next, the ingots with a mass of about 25kg were forged at temperature range from 1200 to 900°C to a thickness of 22 mm. Earlier results (Dobrzański et al., 2009; Grajcar, 2012; Grajcar et al., 2009) indicated that the homogenization annealing followed by hot-forging was enough to fully eliminate the dendritic segregation. Then, cylindrical ∅10x12 mm and cubicoid 15x20x35 mm samples for hot compression tests were prepared by machining. The thermomechanical processing was carried out using the DSI Gleeble 3800 simulator. The specimens were inserted in a vacuum chamber, where they were resistance-heated to a temperature of 1200°C and soaked for 30s. Different plastometric tests were performed to assess the hot-working behavior of investigated steels.

Continuous compression test: To obtain σ-ε curves, the axisymetrical compression tests at the temperatures of 850, 950 and 1150°C with 0.1, 1 and $10s^{-1}$ strain rates were performed. After austenitizing for 30s the specimens were cooled to a deformation temperature and held for 20s before compression to the logarithmic strain of 1 (figure 7).

Double-hit compression test: The softening kinetics of austenite was evaluated by employing the double-hit compression test at a temperature of 900°C and at strain rate of 10 s^{-1} (figure 8). The applied true strain was 0.23 and the holding times between successive compression steps were from 1 to 100 s. The determination of the recrystallized fraction (X) was carried out using the 2% offset method. Some of the samples were water-cooled after applying first compression step to reveal a recrystallization progress by microstructure observations.

Table 1. *Chemical composition of the investigated steels (mass contents, %)*

Generation	Steel grade	C	Mn	Al	Si	Mo	Nb	Ti	S	P
1st	1.5Mn-1Si-0.5Al	0.24	1.55	0.40	0.87	–	0.034	0.023	0.004	0.010
2nd	25Mn-3.5Si-1.5Al	0.054	24.4	1.64	3.49	–	0.029	0.075	0.016	0.004
3rd	3Mn-1.5Al	0.17	3.10	1.50	0.22	0.22	0.040	–	0.005	0.008

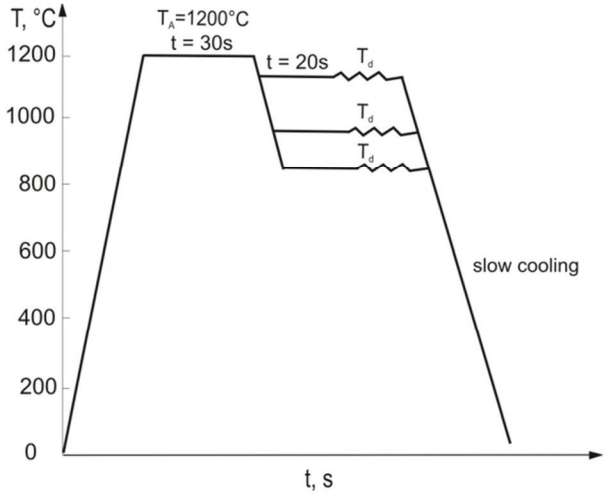

Fig. 7. *Temperature-time-strain conditions of the continuous compression test of axisymetrical specimens.*

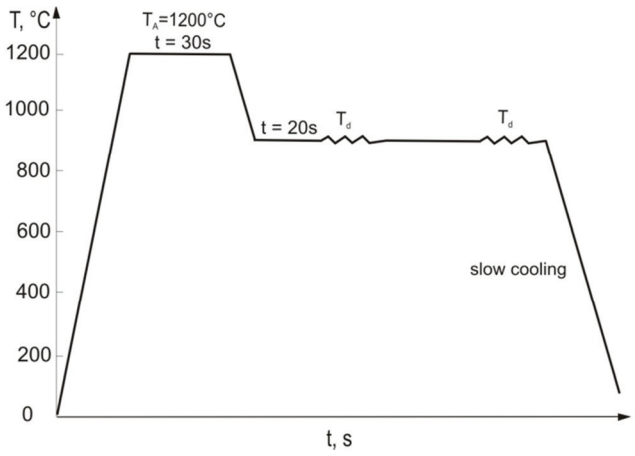

***Fig. 8**. Temperature-time-strain conditions of the double-hit compression test of axisymetrical specimens.*

Four-step compression test: The four-step compression consisted of four deformation steps (1150, 1050, 950, 850°C) of axisymetrical samples according to figure 9. The logarithmic strain value was equal to 0.25 for the low-alloyed steels and 0.29 for the high-Mn steel at the strain rate of $10s^{-1}$ for each deformation step. The detailed temperature-time-strain conditions of hot-working are given in figure 9. Some of the samples were water-cooled after a final deformation step or at different processing stages to reveal a microstructure evolution of austenite. Austenitic steel samples were also solution heat-treated in water from 850°C after the final deformation as well as after various time of isothermal holding of steel at a final compression temperature.

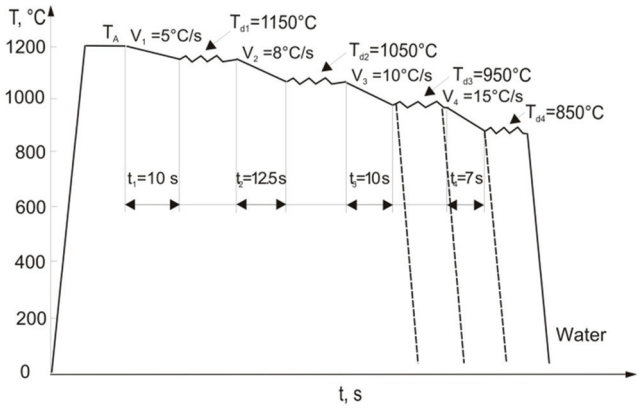

***Fig. 9.** Temperature-time-strain conditions of the four-step compression test of axisymetrical specimens.*

Physical simulation of the thermomechanical processing: Seven-step compression test was carried out for two low-alloyed steels. The deformation schedule (table 2) was designed to reflect an industrial hot strip rolling. After austenitizing at 1200°C for 30s the specimens were cooled to a temperature of first deformation at 1150°C. The strain value for the first compression step and inter-pass time between the first and second deformation steps were high to obtain uniform austenite grains due to dynamic or static recrystallization. Together with lowering deformation temperature the strain rate increases whereas the logarithmic strain and time between successive deformation stages decrease (table 2).

***Table 2.** Parameters of the multi-step compression for cubicoid specimens of 3Mn-1.5Al steel*

Deformation step	Deformation temperature, °C	Logarithmic strain	Strain rate, s^{-1}	Time between deformation steps, s
1	1150	0.4	5	30
2	1000	0.3	5	10
3	950	0.2	10	10
4	900	0.2	10	3
5	870	0.2	30	3
6	860	0.2	50	1
7	850	0.2	50	→700°C

After the final deformation at 850°C the specimens were cooled at a rate of 30°C/s to the temperature of 700°C. Next, the cooling paths differ slightly for two steels for the sake of different chemical composition. The time of slow cooling of 3Mn-1.5Al steel between 700 and 650°C was 10s whereas the 1.5Mn-1Si-0.5Al steel was cooled from 700 to 600°C for 50s (figure 10). Next, the samples were cooled quickly to the bainitic transformation temperature (T_B) of 400°C. The holding time (t_B) for the 1.5Mn-1Si-0.5Al steel was 600s whereas for the 3Mn-1.5Al steel it was twice shorter for the sake of the faster bainitic transformation kinetics in steels containing high Al content. Finally, the specimens were colled at a rate of 0.5°C/s to room temperature (figure 10).

Metallographic specimens were prepared in the plane consistent with the direction of plastic flow. For the purpose of the best identification of retained austenite, etching in 10% water solution of sodium metabisulfite was applied for low-alloyed steels. High-manganese steel samples were etched using 5% nital or a mixture of HNO_3+HCl (2:1). Prior austenite grains were revealed by etching samples in saturated aqueous solution of picric acid with addition of $CuCl_2$. Metallographic observations were carried out using Leica MEF 4A optical microscope at the magnifications from 200x to 1000x. Morpho-

logical features of the microstructure were revealed with the SUPRA 25 scanning electron microscope (SEM).

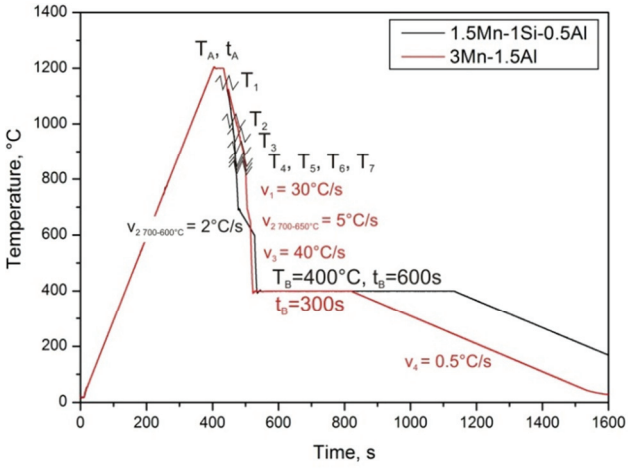

***Fig. 10**. Temperature-time-strain conditions of the multi-step compression test of cubicoid specimens.*

5. RESULTS AND DISCUSSION

5.1. Influence of chemical composition on continuous σ-ε curves

The knowledge of hot deformation resistance of steel is of primary importance for a properly designed thermomechanical rolling of AHSS sheets. Comparison of σ-ε curves obtained for different deformation conditions is shown in figures 11-13. The influence of the deformation temperature and strain rate on a shape of σ-ε curves is typical. Stress values increase with decreasing deformation temperature and increasing strain rate. Dynamic recrystallization is a process controlling work hardening only for the lowest Zener-Holomon parameter values. A clear peak of ε_p (corresponding to a maximum value of flow stress) followed by decreasing flow stress can only be observed for the specimens compressed at a temperature of 1150°C with a strain rate of $0.1s^{-1}$ (figure 11). The 3Mn-1.5Al steel has higher flow stress and critical strain required for initiation of dynamic recrystallization than the 1.5Mn-1Si-0.5Al steel due to the higher total content of alloying elements.

Flow stress increases from 60-70 MPa to 200-220 MPa with lowering the compression temperature from 1150 to 850°C (figure 12). At the same time, values of the ε_p strain shift to higher strains, which are not achievable during hot rolling. A further increase of flow stress of low-alloyed steels up to about 250 MPa can be observed with increasing strain rate to $10s^{-1}$ (figure 13). Stress peaks are not observed on the σ-ε curves, instead the steady state characterized by dynamic equilibrium between work

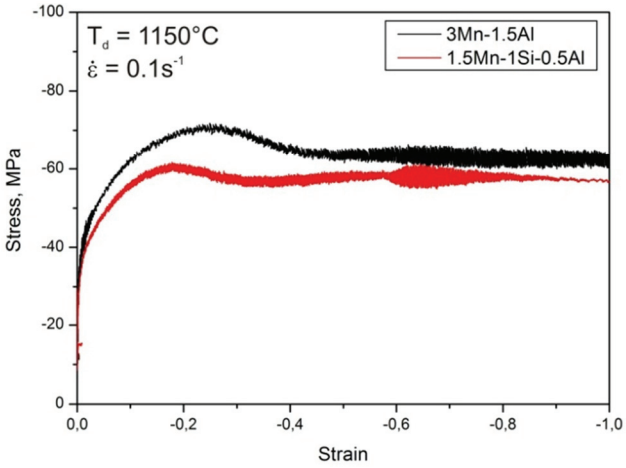

***Fig. 11**. Effect of chemical composition on stress-strain curves obtained at a deformation temperature of 1150°C and strain rate of 0.1 s^{-1}.*

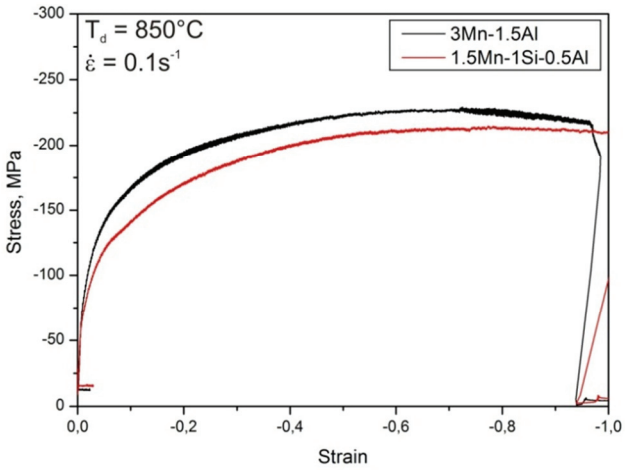

***Fig. 12.** Effect of chemical composition on stress-strain curves obtained at a deformation temperature of 850°C and strain rate of 0.1 s^{-1}.*

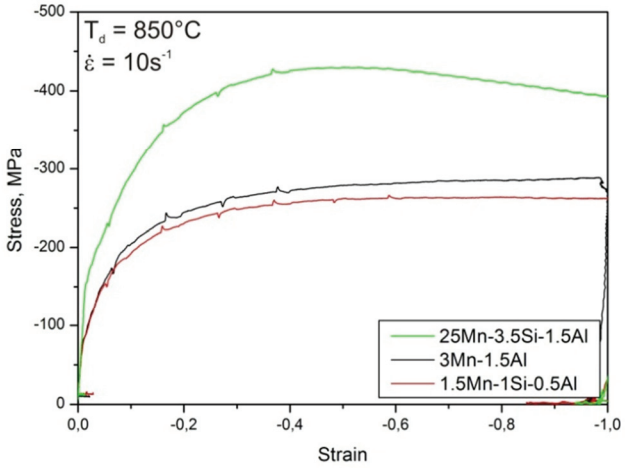

***Fig. 13.** Effect of chemical composition on stress-strain curves obtained at a deformation temperature of 850°C and strain rate of 10 s^{-1}.*

hardening and its removal by dynamic recovery occurs in a very wide range of strain. The different shape of the σ-ε curve is present for the high-Mn steel. It strengthens considerably at the initial stage of deformation and after rising a critical strain (ε_p), flow stress decreases as a result of dynamic recrystallization. The hot working of the high-Mn steel is more difficult due to considerably higher flow stresses required, what is a direct effect of high Mn alloying.

5.2. Influence of chemical composition on softening kinetics of austenite

Softening kinetics curves are very useful to assess the extent of recrystallization between successive deformation stages and potential residual strain. An exemplary set of σ-ε curves for the 3Mn-1.5Al steel, obtained on the basis of the double-hit compression tests is shown in figure 14. It is typical that with increasing the holding time at 900°C, a shape of σ-ε curve determined for a second deformation step is more and more similar to a shape of the first curve. It corresponds to a progress of the static recovery and recrystallization. Flattening of the curves corresponding to short inter-deformation time can be an indication of the lack of dynamic recovery of strain accumulated from the first deformation step.

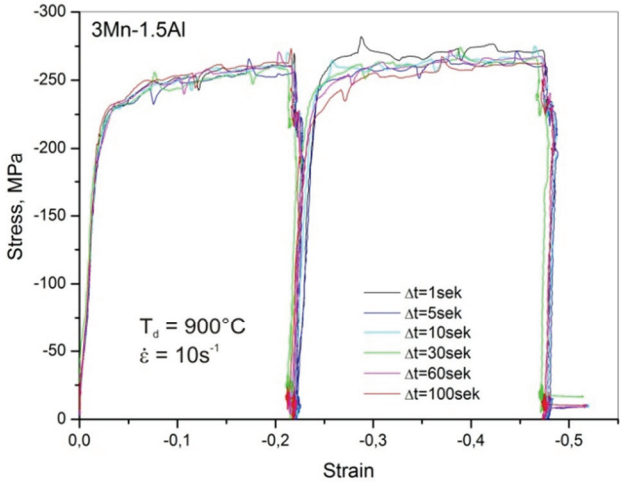

Fig. 14. Stress-strain curves obtained during the double-hit compression test of 3Mn-1.5Al steel for different inter-deformation time.

Figure 15 compares the change of the softening fraction (X) as a function of time for all three steels investigated. The data can be relatively well fitted with the sigmoidal curves, corresponding to the Avrami-type relationship. It is interesting to note that the softening kinetics of the 25Mn-3.5Si-1.5Al steel is much faster compared to low-alloyed steels. It is strictly related to the effect of Mn on the hot-working behavior. Cabanas et al. (2006) investigated the influence of Mn content on the hot deformation resistance of Fe-Mn alloys containing from 1 to 20 wt.% Mn. It has been found that the activation energy of hot-working increased with increasing Mn content but only for Mn contents <10%, where manganese was found to delay dynamic recrystallization. At higher Mn contents (>10 wt.% Mn) a decrease in the activation energy was observed. It indicates that the strengthening effect of Mn is limited to medium levels of Mn alloying and the hot deformation resistance of high-Mn steels is probably dependent on the stacking fault energy (SFE), similarly to its effect on a major deformation mechanism during cold straining. This indicates a complex effect of Mn on the hot-working behavior of AHSS steels and requires further research. Anyway, the 50%-recrystallized fraction of austenite occurs for the $t_{0.5}$ time equal to about 20s (figure 15). A similar relatively fast course of static recrystallization was observed by Hamada et al. (2007) in 25Mn and 25Mn(1-3)Al alloys, where their softening kinetics was faster compared to 304-type austenitic and C-Mn-Nb microalloyed steels. The statically recrystallized austenite fraction increasing as a function of isothermal holding time at a deformation temperature of 900°C revealed after etching (figure 16) corresponds well with a softened fraction determined on a basis of double-hit compression test (figure 15).

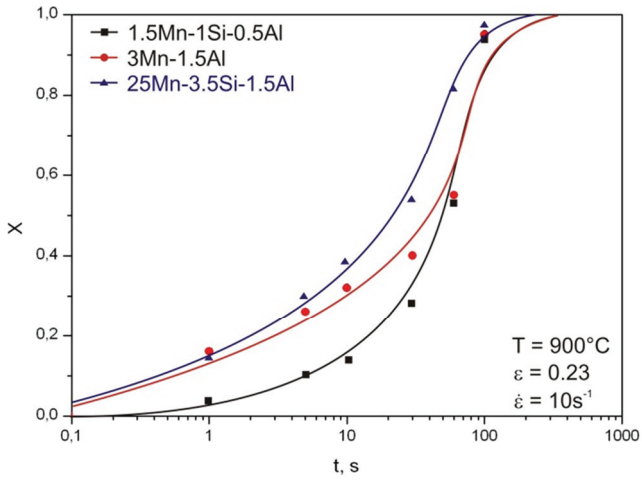

Fig. 15. Effect of chemical composition on a softening fraction of austenite.

Time of half-recrystallization extends to about 30 and 40s, respectively for the steels containing 3 and 1.5% Mn (figure 15). Again, it is interesting that the recrystallization progress of 3Mn-1.5Al steel is faster than that of 1.5Mn-1Si-0.5Al steel. It can be

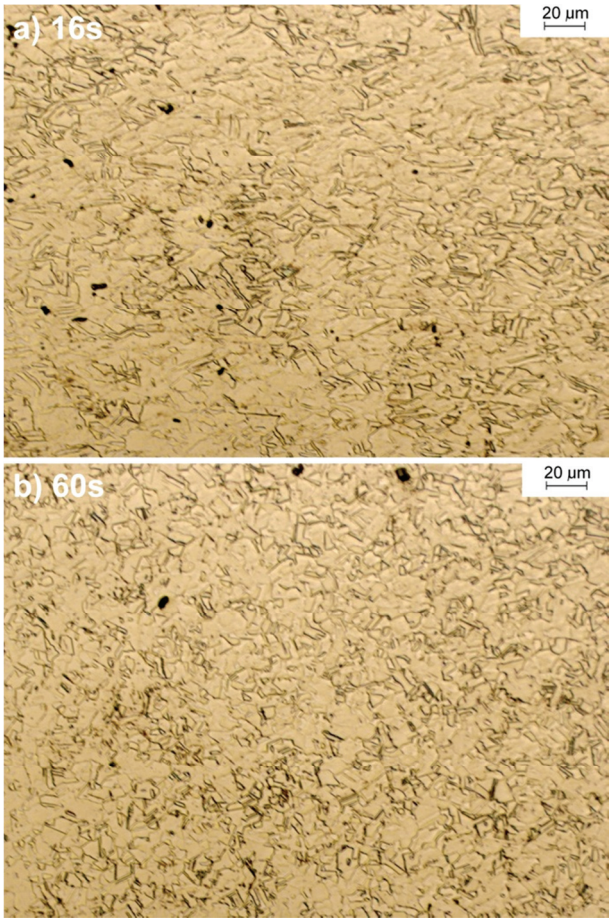

Fig. 16. *Partially statically recrystallized austenite grains of the high-Mn steel solution heat-treated after isothermal holding of steel at a deformation temperature of 900°C for 16s (a) and 60s (b).*

explained by the interaction between Nb microaddition and other alloying elements. During considering the effect of Nb it is required to distinguish between Nb in solid solution and Nb present as Nb(C,N) particles. The solute drag effect acting on the moving grain boundaries and the particle pinning can retard or even prevent the occurrence of recrystallization. It is well known (Poliak & Siciliano, 2004) that increasing the Mn content in Nb-microalloyed steels significantly delays the precipitation of Nb(C,N). Manganese increases the solubility of NbC and NbN in austenite, decreases Nb diffusivity and finally retards the rate of precipitation of Nb(C,N). Moreover, Al alloying acts in the same direction as Mn because Al suppresses precipitation of Nb(C,N) during hot-working due to strong affinity of Al to nitrogen (Skolly & Poliak, 2005). By contrast, Si addition has an accelerating effect. It means that the precipitation process of Nb(C,N) in the steel containing 1% Si and low contents of Mn and Al is faster and prevents a static recrystallization progress more effectively compared to the 3Mn-1.5Al steel (figure 15). Additionally, the austenite grain boundary migration of the 1.5Mn-1Si-0.5Al steel is hampered by TiN particles. Successive stages of a recrystallization progress for the 1st generation AHSS are shown in figure 17. After 20s isothermal holding the flattened statically recovered grains of austenite are mainly visible (figure 17a), whereas a mixture of fine recrystallized grains and larger recovered grains can be observed after 40s (figure 17b).

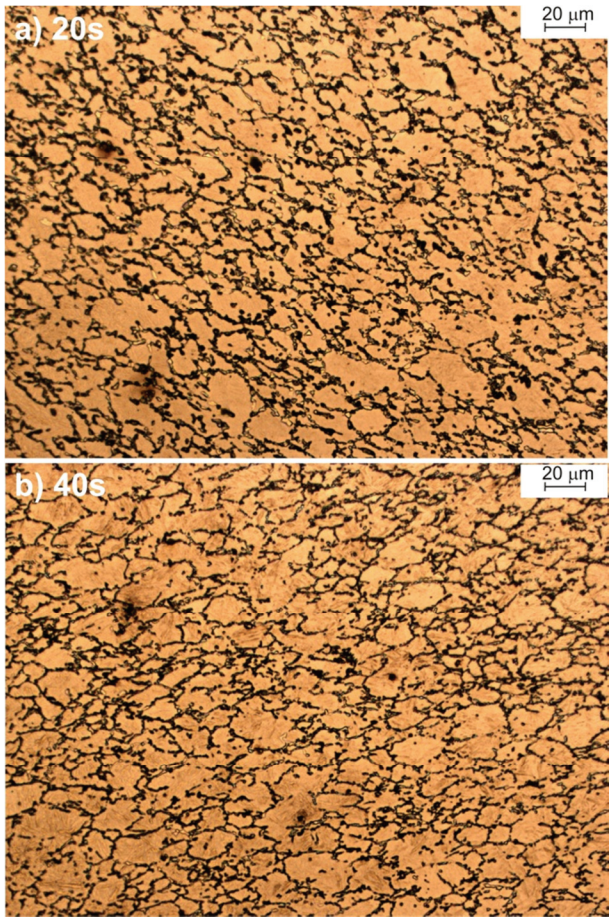

Fig. 17. *Partially statically recrystallized austenite grains of the 1.5Mn-1Si-0.5Al steel water-quenched after isothermal holding of steel at a deformation temperature of 900°C for 20s (a) and 40s (b).*

5.3. Influence of chemical composition on the hot-working behavior during four-step compression

A result of the four-step compression according to figure 9 are the σ-ε curves in figure 18. The values of flow stress for all the steels increase significantly with decreasing the deformation temperature. Final flow stresses registered at a deformation temperature of 850°C are similar to those obtained during continuous compression for two low-alloyed steels, whereas they are smaller for the high-Mn steel. Generally, it can be concluded that thermally activated processes of microstructure restoration

occurring during inter-deformation time proceed faster in the high-alloyed steel. Anyway, the flow stress is the highest for the austenitic steel in a whole range of hot-working and decreases in the same order as described above, i.e., 3Mn-1.5Al and 1.5Mn-1Si-0.5Al. The dynamic recovery is a process controlling work hardening and subsequent flow stresses for the whole deformation temperature range for two low-alloyed steels. Taking into account the strain values, strain rate and deformation temperature applied it can be expected that during two initial inter-deformation times a recrystallized fraction is higher than 50% and about 20% during cooling between third and fourth deformation steps. The confirmation of the successive grain refinement of the 1.5Mn-1Si-0.5Al steel due to repeated recrystallization are the micrographs in figure 19 showing prior austenite grain boundaries. Cooling the steel for 7s between the third and the fourth compression steps leads to a partially statically recrystallized microstructure of austenite with an average grain size of approximately 18 μm (figure 19a). After the final deformation at a temperature of 850°C, the fine-grained pancaked microstructure of slightly elongated austenite grains with a diameter of about 12 μm can be observed (figure 19b). It confirms that austenite recrystallized just partially between final deformation steps and is highly defected before successive multi-step cooling.

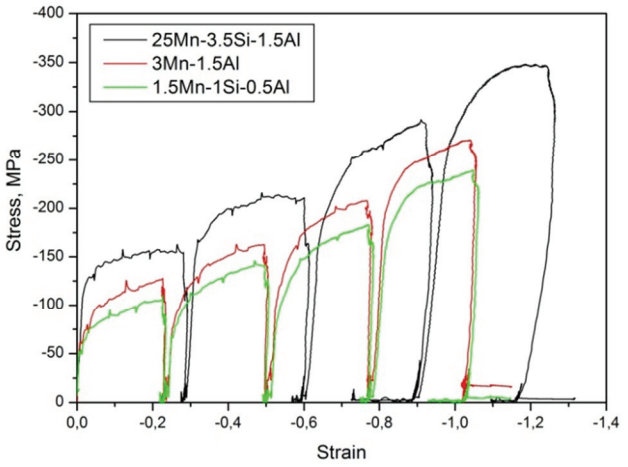

Fig. 18. *Effect of chemical composition on σ-ε curves obtained during four-step compression.*

A different shape of σ-ε curves in figure 18 can be observed for the high-Mn steel. There are two peaks present on the two initial registered curves indicating the initiation of dynamic recrystallization. Hence, the metadynamic followed by static recrystallization should proceed during the inter-deformation time resulting in a progressive grain refinement. A microstructure evolution of the high-Mn steel is presented in figure 20. Equiaxial recrystallized austenite grains with a diameter of about 30 μm are present just before the third deformation step (figure 20a). Many annealing twins and plates of ε martensite (identified elsewhere by Grajcar et al., 2009) are also visible. Lowering the deformation temperature to 950°C results in decreasing austenite grain size to about 20 μm. A ε_p peak is not present during compression at 950°C, hence a successive grain refinement occurring between two final deformation steps proceeds because of static recrystallization. As a result a mixture of elongated statically recovered grains and fine recrystallized grains is revealed (figure 20b).

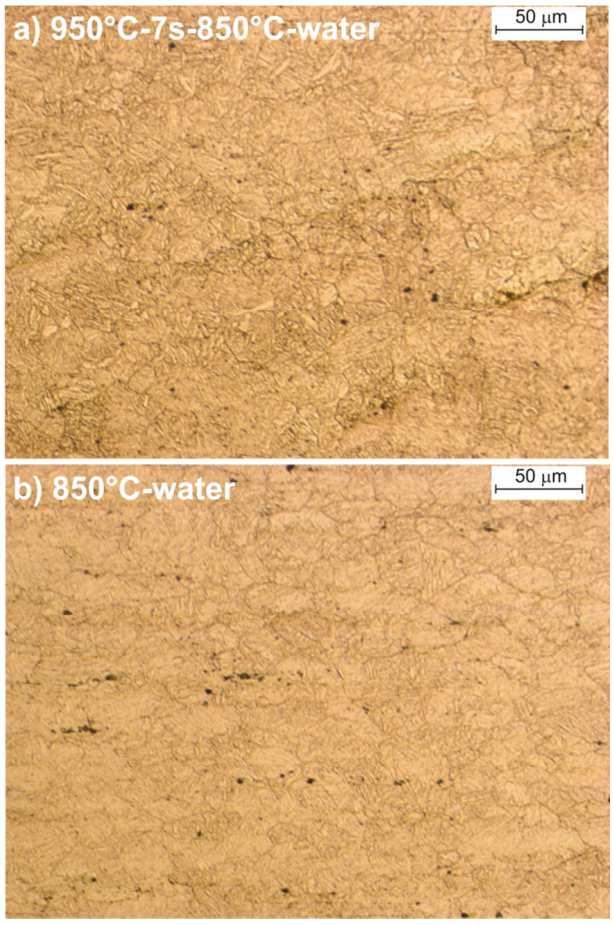

Fig. 19*. Prior austenite grain boundaries of the 1.5Mn-1Si-0.5Al steel before the last compression step (a) and after the last deformation at 850°C.*

The relatively short inter-deformation time and a subsequent small fraction of recrystallized grains lead to residual strain summing with the strain value applied during the final compression step. The accumulated strain leads to initiation of dynamic recrystallization revealing as a stress peak on the final σ-ε curve (figure 18). Finally, after the last deformation

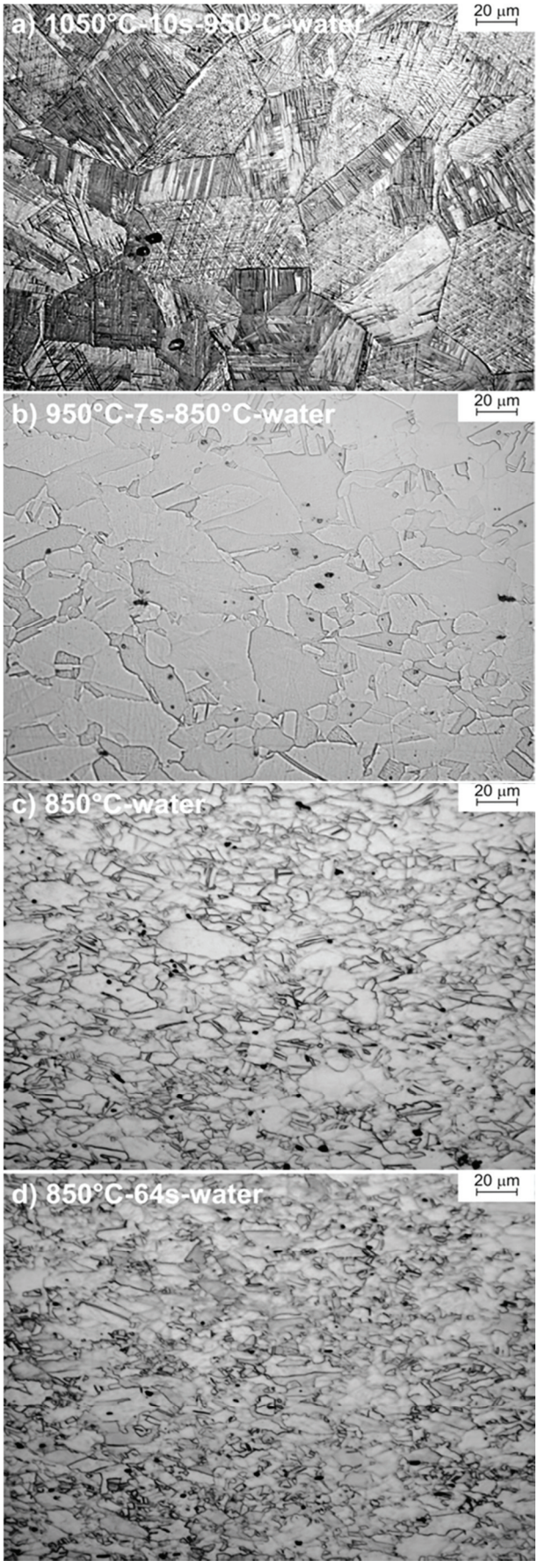

Fig. 20. Successive stages of microstructure evolution of the high-Mn steel solution heat-treated at different stages of four-step compression.

steel possesses the fine-grained microstructure composed of dynamically recovered elongated grains and a large fraction of dynamically recrystallized fine grains (figure 20c). Isothermal holding of steel at 850°C up to 64s leads to a further microstructure refinement due to a progressive course of recrystallization. A final recrystallized grain size covers a range from 5 to 10 µm (figure 20d). The substantial contribution of thermally activated processes removing work hardening during multi-step compression decreases the flow stress compared to continuous compression conditions (figure 13) and makes possible to obtain very fine-grained microstructure products.

5.4. Physical simulation of thermomechanical processing

Physical simulation of thermomechanical processing yielded the σ-ε curves in figure 21. The values of flow stress for two low-alloyed steels increase significantly with decreasing the deformation temperature. They are about 100 MPa higher compared to these ones registered during four-step compression (figure 18) due to strain accumulation and higher strain rates applied at final deformation stages. It appears on a basis of the shape of σ-ε curves that dynamic recovery is a process controlling work-hardening for the overall temperature range of hot-working. Therefore, the microstructure evolution of austenite is dependent on a partial static recrystallization progress between successive deformation steps. As earlier, the steel containing 3% Mn has higher flow stress values than the 1.5Mn-1Si-0.5Al steel (figure 21).

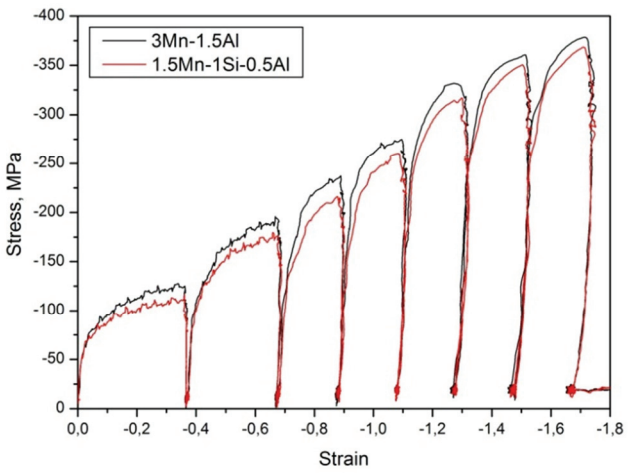

Fig. 21. Effect of chemical composition on σ-ε curves obtained during multi-step compression of specimens under conditions of plane state of strain.

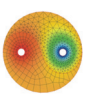

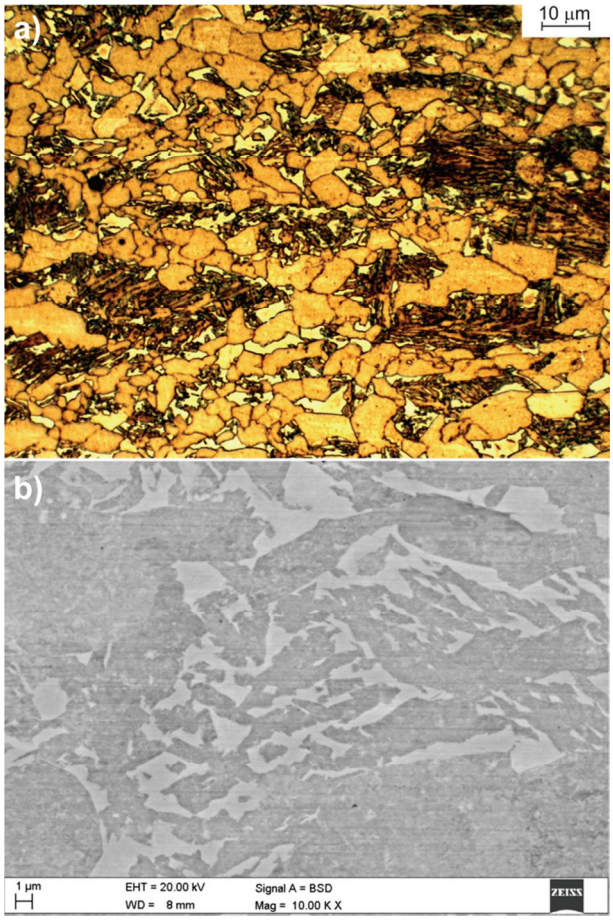

Fig. 22. *Fine-grained ferritic-bainitic microstructure containing blocky-type and interlath retained austenite of the 1.5Mn-1Si-0.5Al steel (a) and morphological features of retained austenite forming the BA (bainitic austenitic) island (b).*

Stress-strain curves for the high-Mn steel were not registered but it is expected on a basis of presented above data that flow stress should be the highest of all the steels investigated. It is confirmed by stress-strain data reported by Dobrzański and Borek (2012) for the 25Mn-3Al-1Si-Nb-Ti steel, where flow stresses at a final deformation temperature of the thermomechanical treatment approach 400 MPa.

As a result of the thermomechanical processing performed the fine-grained ferritic-bainitic microstructure with a ferrite fraction of about 60% and high amount of retained austenite was obtained for the 1st generation AHSS (figure 22). The amount of γ phase determined by X-ray is about 14%. Enrichment of austenite in carbon during the γ→α transformation and following isothermal holding of samples at a temperature of 400°C leads to lowering the martensite start of γ phase below room temperature. A mean ferrite grain size is equal to 6µm and retained austenite is located on ferrite boundaries as blocky grains with a size up to 5 µm (figure 22a). A part of retained austenite grains forms a continuous or interrupted layer around α phase grains whereas the rest is located on ferrite-bainite interfaces. A large fraction of γ phase as thin layers or fine blocky grains with a size between 1 and 3µm is a constituent of bainitic islands (BA) (figure 22b).

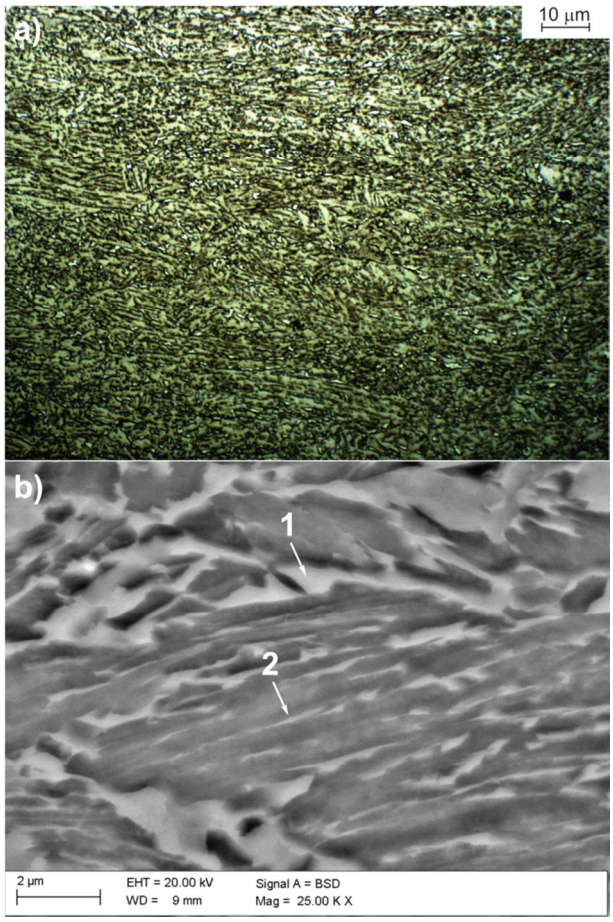

Fig. 23. *Fine-grained bainitic-martensitic microstructure containing granular (1) and interlath (2) retained austenite of the 3Mn-1.5Al steel (a) and morphological features of retained austenite (b).*

Even more fine-grained microstructure was obtained for the 3rd generation AHSS (figure 23). A lath bainitic-martensitic microstructure is a result of the higher hardenability of the 3Mn-1.5Al steel. A small fraction of ferrite can also be observed. A fraction of retained austenite is equal to about 17%. Retained austenite is uniformly distributed in a bainitic matrix and two main morphologies of this phase can be distinguished – granular and interlath retained austenite (figure 23b). Layers of retained austenite located between bainitic ferrite laths instead of cementite form the microstructures similar to degenerated upper bainite (Zajac et al., 2005). A size of γ grains does not exceed 2 µm but a majority of them has a diameter smaller than about 1 µm, what favours their stabilization. Some larger blocky

austenite regions transformed into martensite during a final slow cooling but their fraction is very low.

6. SUMMARY

The hot-working behaviour and microstructure evolution of austenite during successive deformation stages as well as its transformation products formed during controlled cooling for different AHSS grades are compared in the present work. It has been shown that it is possible to obtain very fine-grained ferrite-based, bainite-based or austenite-based microstructures depending on a steel grade and cooling path applied. A very important structural constituent of investigated low-alloyed AHSS is retained austenite. After controlled cooling its amount reaches from 14 to 17% and retained austenite is present as blocky grains, granules or thin layers forming microstructures similar to degenerate upper bainite. It was proved that the presence of γ phase at room temperature requires its size stabilization by grain refinement due to the strong effect of Mn on hardenability of austenite and its tendency to martensitic transformation. The single-phase austenitic microstructure was formed in the investigated high-Mn steel without special attention to cooling procedures. However, this steel is characterized by the highest hot deformation resistance due to the high content of Mn, Al and Si. As distinct from the low-alloyed steels, its grain refinement can be done utilizing dynamic recrystallization, whereas a microstructure evolution of low-alloyed steels is controlled by dynamic recovery and a partial progress of static recrystallization between successive deformation steps. Force-energetic parameters of hot-working decrease with decreasing content of alloying elements and they are the lowest for the 1st generation AHSS.

ACKNOWLEDGEMENTS

The work was partially supported by the Polish Ministry of Science and Higher Education in a period of 2010-2012 in the framework of project No. N N508 590039.

REFERENCES

Adamczyk, J., Grajcar, A., 2007, Heat treatment and mechanical properties of low-carbon steel with dual-phase microstructure, *Journal of Achievements in Materials and Manufacturing Engineering*, 22, 13-20.

Bleck, W., Phiu-On, K., 2005, Microalloying of cold-formable multi phase steel grades, *Materials Science Forum*, 500-501, 97-112.

Cabanas, N., Akdut, N., Penning, J., De Cooman, B.C., 2006, High-temperature deformation properties of austenitic Fe-Mn alloys, *Metallurgical and Materials Transactions A*, 37A, 3305-3314.

Dobrzański, L.A., Borek, W., 2012, Thermo-mechanical treatment of Fe-Mn-(Al,Si) TRIP/TWIP steels, *Archives of Civil and Mechanical Engineering*, 12, 299-304.

Dobrzański, L.A., Grajcar, A., Borek, W., 2009, Processes forming the microstructure evolution of high-manganese austenitic steel in hot-working conditions, *Journal of Achievements in Materials and Manufacturing Engineering*, 37, 9-19.

Eberle, K., Cantinieaux, P., Harlet, P., 1999, New thermomechanical strategies for the production of high strength low alloyed multiphase steel showing a transformation induced plasticity (TRIP) effect, *Steel Research*, 70, 233-238.

Ehrhardt, B., Gerber, T., 2004, Property related design of advanced cold rolled steels with induced plasticity, *Steel Grips*, 4, 247-255.

Fazeli, F., Militzer, M., 2012, Modelling simultaneous formation of bainitic ferrite and carbide in TRIP steels, *ISIJ International*, 52, 650-658.

Frommeyer, G., Bruex, U., 2006, Microstructures and mechanical properties of high-strength Fe-Mn-Al-C light-weight TRIPLEX steels, *Steel Research International*, 77, 627-633.

Grajcar, A., 2007a, Determination of the stability of retained austenite in TRIP-aided bainitic steel, *Journal of Achievements in Materials and Manufacturing Engineering*, 20, 111-114.

Grajcar, A., 2007b, Effect of hot-working in the $\gamma+\alpha$ range on a retained austenite fraction in TRIP-aided steel, *Journal of Achievements in Materials and Manufacturing Engineering*, 22, 79-82.

Grajcar, A., 2012, Segregation behaviour of third generation advanced high-strength Mn-Al steels, *Archives of Foundry Engineering*, 24, 123-128.

Grajcar, A., Kuziak, R., Zalecki, W., 2012, Third generation of AHSS with increased fraction of retained austenite for the automotive industry, *Archives of Civil and Mechanical Engineering*, 12, 334-341.

Grajcar, A., Opiela, M., Fojt-Dymara, G., 2009, The influence of hot-working conditions on a structure of high-manganese steel, *Archives of Civil and Mechanical Engineering*, 9, 49-58.

Gronostajski, Z., Niechajowicz, A., Polak, S., 2010, Prospects for the use of new-generation steels of the AHSS type for collision energy absorbing components, *Archives of Metallurgy and Materials*, 55, 221-230.

Hadasik, E., Kuziak, R., Kawalla, R., Adamczyk, M., Pietrzyk, M., 2006, Rheological model for simulation of hot rolling of new generation steel strip for automotive industry, *Steel Research International*, 77, 927-933.

Hamada, A.S., Somani, M.Ch., Karjalainen, L.P., 2007, High temperature flow stress and recrystallization behavior of high-Mn TWIP steels, *ISIJ International*, 47, 907-912.

Koistinen, D.P., Marburger, R.E., 1959, A general equation prescribing extent of austenite-martensite transformation in pure Fe-C alloys and plain carbon steels, *Acta Metallurgica*, 7, 59-60.

Kuc, D., Gawąd, J., 2011, Modelling of microstructure changes during hot deformation using cellular automata, *Archives of Metallurgy and Materials*, 56, 523-532.

Kuziak, R., 2005, *Modelling of structure and phase transformation changes occurring during thermomechanical processing of steel*, Instytut Metalurgii Żelaza, Gliwice (in polish).

Kuziak, R., Kawalla, R., Waengler, S., 2008, Advanced high strength steels for automotive industry, *Archives of Civil and Mechanical Engineering*, 8, 103-118.

Kuziak, R., Molenda, R., Radwański, K., 2011, Modelling of phase transformations during annealing of DP steel sheets using Thermocalc and Dictra software, *Prace IMŻ*, 3, 7-20 (in Polish).

Kuziak, R., Pietrzyk, M., 2011, Physical and numerical simulation of the manufacturing chain for the DP steel strips, *Steel Research International, Special Edition: Technology of Plasticity*, 756-761.

Liu, D., Fazeli, F., Militzer, M., Poole, W.J., 2007, A microstructure evolution for hot rolling of a Mo-TRIP steel, *Metallurgical and Materials Transactions A*, 38A, 894-909.

Majta, J., Kuziak, R., Pietrzyk, M., 1998, Modelling of the influence of thermomechanical processing of Nb-microalloyed steel on the resulting mechanical properties, *Journal of Materials Processing Technology*, 80-81, 524-530.

Militzer, M., 2000, Modelling of microstructure evolution and properties of low-carbon steels, *Acta Metallurgica Sinica*, 13, 574-580.

Militzer, M., 2007, Computer simulation of microstructure evolution in low carbon sheet steels, *ISIJ International*, 47, 1-15.

Militzer, M., Hawbolt, E.B., Meadowcroft, T.R., 2000, Microstructural model for hot strip rolling of high-strength low-alloy steels, *Metallurgical and Materials Transactions A*, 31A, 1247-1259.

Molenda, R., Kuziak, R., Pidvysotsk'yy, V., 2010, Physical simulation and mathematical modeling of rolling and continuous annealing of DP strips, *Prace IMŻ*, 1, 136-141 (in Polish).

Niżnik, B., Pietrzyk, M., 2011, Model of phase transformation for niobium microalloyed steels, *Archives of Metallurgy and Materials*, 56, 731-742.

Opiela, M., Grajcar, A., Krukiewicz, W., 2009, Corrosion behaviour of Fe-Mn-Si-Al austenitic steel in chloride solution, *Journal of Achievements in Materials and Manufacturing Engineering*, 33, 159-165.

Pietrzyk, M., Madej, Ł., Rauch, Ł., Gołąb, R., 2010, Multiscale modelling of microstructure evolution during laminar cooling of hot rolled DP steel, *Archives of Civil and Mechanical Engineering*, 10, 57-67.

Poliak, E.I., Siciliano, F., 2004, Hot deformation behavior of Mn-Al and Mn-Al-Nb steels, *Conf. Proc. MS&T'2004*, New Orleans, USA, AIST, 39-45.

Siodlak, D., Lotter, U., Kawalla, R., Schwich, V., 2008, Modelling of the mechanical properties of low alloyed multiphase steels with retained austenite taking into account strain-induced transformation, *Steel Research International*, 79, 776-783.

Skolly, R.M., Poliak, E.I., 2005, Aspects of production hot rolling of Nb microalloyed high Al high strength steels, *Materials Science Forum*, 500-501, 187-194.

Speer, J.G., De Moor, E., Findley, K.O., Matlock, D.K., De Cooman, B.C., Edmonds, D.V., 2011, Analysis of microstructure evolution in quenching and partitioning automotive sheet steel, *Metallurgical and Materials Transactions A*, 42A, 3591-3601.

Suwanpinij, P., Prahl, U., Bleck, W., Kawalla, R., 2012, Fast algorithms for phase transformations in dual phase steels on a hot strip mill run-out table (ROT), *Archives of Civil and Mechanical Engineering*, 12, 305-311.

Thomas, G.A., Speer, J.G., Matlock, D.K., 2011, Quenched and partitioned microstructures produced via Gleeble simulations of hot-strip mill cooling practices, *Metallurgical and Materials Transactions A*, 42A, 3652-3659.

Uranga, P., Lopez, B., Rodriguez-Ibabe, J.M., 2007, Microstructural modeling of Nb microalloyed steels during thin slab direct rolling processing, *Steel Research International*, 78, 199-209.

Zajac, S., Schwinn, V., Tacke, K.H., 2005, Characterisation and quantification of complex bainitic microstructures in high strength coated sheet steels, *Materials Science Forum*, 500-501, 387-394.

SYMULACJA FIZYCZNA OBRÓBKI CIEPLNO-PLASTYCZNJ NOWEJ GENERACJI STALI WYSOKOWYTRZYMAŁYCH

Streszczenie

Celem naukowym pracy jest analiza porównawcza obróbki plastycznej na gorąco i rozwoju mikrostruktury obrobionych cieplno-plastycznie oraz chłodzonych w kontrolowanych warunkach trzech wysokowytrzymałych stali stosowanych w motoryzacji (AHSS). Przedstawiono porównanie odkształcalności na gorąco 3 wybranych gatunków stali o zróżnicowanej zawartości Mn i C, będących głównymi pierwiastkami austenitotwórczymi. Oceny oporu kształtowania plastycznego dokonano na podstawie prób ściskania ciągłego, ściskania dwuetapowego, czteroetapowego oraz siedmioetapowego symulującego warunki zbliżone do procesów przemysłowych. Stwierdzono, że odkształcalność na gorąco nowej generacji stali AHSS wymaga zastosowania dużej wartości naprężeń uplastyczniających. Możliwe jest jednak uzyskanie drobnoziarnistych produktów przemiany austenitu przechłodzonego o dużym udziale austenitu szczątkowego w stalach niskostopowych lub jednorodnej strukturze austenitycznej w stali wysokomanganowej. Dokonano identyfikacji aktywowanych cieplnie procesów odbudowy mikrostruktury austenitu pozwalających na sukcesywne jego rozdrobnienie oraz decydujących o końcowej wartości naprężenia płynięcia. Porównano uzyskane mikrostruktury stali charakteryzujące pierwszą, drugą i trzecią generację stali AHSS. Wskazano podobieństwa i różnice dotyczące odkształcalności stali na gorąco oraz szczegółów mikrostrukturalnych.

Received: October 5, 2012
Received in a revised form: November 25, 2012
Accepted: December 3, 2012